Design of slit width to improve space harmonic distribution in a slit stator motor

Yuichi Yokoi[1]*, Ryuta Hashizume[1], Tsuyoshi Higuchi[1]

[1] *Graduate School of Engineering, Nagasaki University, Nagasaki, Japan*
* *E-mail: yyokoi@nagasaki-u.ac.jp*

Abstract: This paper designs the width of slit-like flux barriers to improve the space harmonic distribution of the air-gap flux density in a slit stator motor. The slit stator motor has slit-like flux barriers at wound teeth of the stator. The stator design can adjust the space harmonic distribution with the slit width. Space harmonic distributions govern torque and losses in motors. For this reason, the dependence of the space harmonic distribution on the slit width should be clarified to design slit stator motors. The dependence is investigated through a theoretical calculation based on a magnetic circuit model and a finite element method analysis. These methods show that a space harmonic producing the drive torque is maximised at a slit width and other dominant detrimental space harmonics are decreased with the increase of the slit width. The improved space harmonic distribution is verified by performing an experiment with a measuring rotor.

1 Introduction

Space harmonic distribution of magnetic flux density across the air gap governs torque and losses in electrical machines [1–5]. Fractional-slot concentrated winding configurations generate several dominant space harmonics. One of them produces the drive torque. The others increase undesirable effects such as iron loss in cores and eddy-current loss in magnets without contributing to torque production. In the design of fractional-slot concentrated winding machines, the space harmonic distribution can be improved with many design methods such as multilayer winding configurations whose number of layers is greater than two [6–12] and several stator core structures [13–17].

A slit stator motor has been proposed to improve the space harmonic distribution of the air-gap flux density for 12-slot 10-pole motors [18][19]. In the motor, the stator has slit-like flux barriers at alternate teeth. The stator winding coils are wound around the slit teeth. This stator design increases the space harmonic producing the drive torque and decreases dominant space harmonics generating losses. As a result, the slit stator motor achieves higher torque production and efficiency than a conventional motor.

In the design of slit stator motors, the width of the slit-like flux barriers is the most essential design parameter. The slit width governs the space harmonic distribution. The effect of the slits to barrier magnetic flux across them is enhanced with the increase of the slit width. However, the net width of stator teeth and/or the area of slots decrease as the slit width increases within a sectional area of the stator. In addition, the flux density drops in the air gap on the slits. This can change the space harmonic distribution. In [17], the influence of the width of flux gaps, which correspond to slits in unwound teeth, on the space harmonic for the drive torque is investigated for 12-slot machines. Therefore, the dependence of the space harmonic distribution on the slit width should be clarified to design slit stator motors.

In this paper, the width of the slit-like flux barriers is designed to improve the space harmonic distribution of the air-gap flux density in a slit stator motor [20]. The influence of the slit width on the space harmonic distribution is investigated through a theoretical calculation based on a magnetic circuit model and a finite element method (FEM) analysis. The improved space harmonic distribution is verified experimentally.
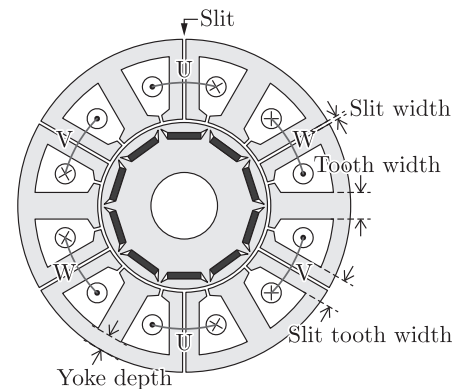
Fig. 1: Cross section of a slit stator motor

Table 1 Dimensions of the conventional and the slit stator motors

		Conventional	Slit stator
Stack length	L	50 mm	50 mm
Stator outer diameter	d_s	160 mm	160 mm
Rotor outer diameter	d_r	88 mm	88 mm
Air gap length	l_g	1 mm	1 mm
Tooth width		15.5 mm	15.5 mm
Slit tooth width		—	15.5 mm + w
Slit width	w	—	w
Yoke depth		10 mm	7.8 mm
Number of turns per coil	N_{coil}	80	80

2 Slit Stator Motor

This section briefly describes the structure, the air-gap flux density distribution, and the performance of a slit stator motor in comparison with a conventional motor through a 2-dimensional (2D) FEM analysis. The slit width is fixed at $w = 1.0\,\mathrm{mm}$ as an example in this section.

Figure 1 shows the cross section of a slit stator motor. The motor configures a 12-slot 10-pole permanent magnet motor with single-layer windings. Slit-like flux barriers are located at the centre of the wound teeth in the stator. The dimensions of the slit stator motor and a conventional motor are presented in Table 1. The width of teeth
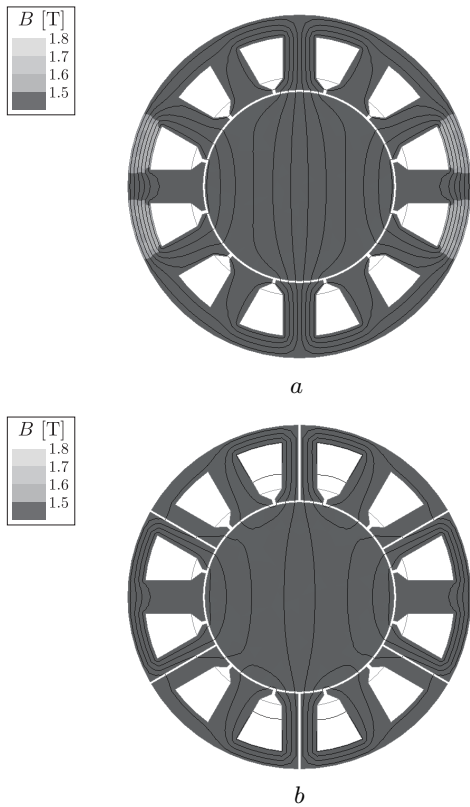
Fig. 2: Distribution of magnetic flux and its density at a fed current of 10 A with maximising the U-phase current in the conventional motor and the slit stator motor with a slit width of 1 mm

a Conventional
b Slit stator

Fig. 3: Air-gap flux density at a fed current of 10 A with maximising the U-phase current in the conventional motor and the slit stator motor with a slit width of 1 mm

a Spatial distribution
b Harmonic components

with slits is greater than that of teeth without slits by the slit width. This implies that all the teeth have an identical width of iron core not to enhance magnetic saturation in the slit teeth. The depth of the stator yoke in the slit stator motor can be less than that in the conventional motor. In the slit stator motor, the yoke depth is set at half of the tooth width. This is based on the assumption that the magnetic flux across the slits should be completely suppressed. In the conventional motor, the yoke depth should be greater than half of the tooth width. The wider yoke allows some of the magnetic flux that goes straight on the yoke at the intersections with wound teeth.

The distribution of magnetic flux and its density due to a stator winding current is influenced by the slit-like flux barriers, as shown in Fig. 2. The fed current is set at 10 A and the phase is adjusted to maximise the U-phase current on the field oriented control. In the FEM analysis, the rotors are modelled as iron cores that do not have shafts, magnets, or magnet insertion holes to remove the influence of the rotor structure. In comparison with the conventional motor, the slit stator motor exhibits more flux loops around only a slot. This corresponds to the increase of space harmonics whose wavelength is approximately equal to twice the slot pitch, namely, the 5th and/or the 7th space harmonics. The number of flux loops that flow near the centre of the rotor core is decreased by the slits. This corresponds to the decrease of the fundamental space harmonic. In addition, the magnetic flux density is decreased at the yoke by the slits. The slits can suppress the magnetic saturation in cores.

The distribution of the air-gap flux density is modified with the slit-like flux barriers. Fig. 3 shows the spatial distribution of the air-gap flux density due to a stator winding current and its harmonic components for the magnetic flux distribution shown in Fig. 2. Fig. 3a shows that the slits change the spatial distribution of the air-gap flux density. In particular, the flux density differs on the sides of slits for the teeth at $30°$, $150°$, $210°$, and $330°$. The slits increase the 5th space harmonic and decrease the fundamental and 7th space harmonics, as shown in Fig. 3b. In conventional 12-slot 10-pole motors,
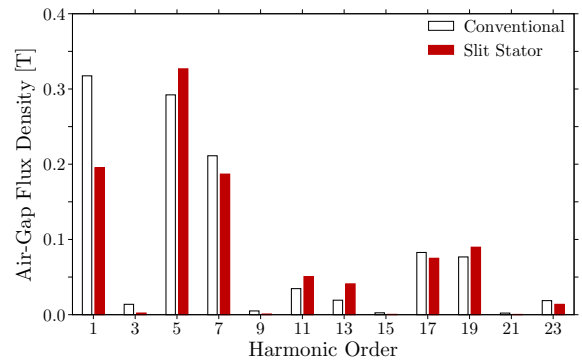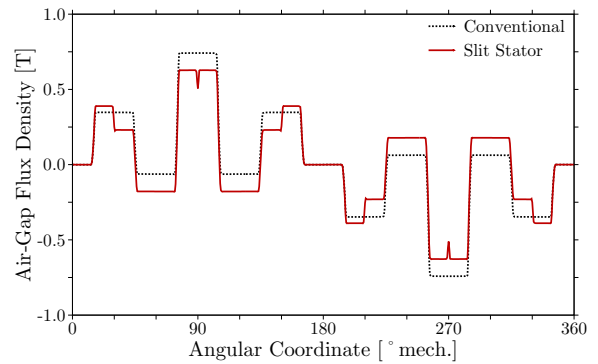
Table 2 Performance of the conventional motor and the slit stator motor with a slit width of 1 mm

	Conventional	Slit stator
Current	10.0 A	10.0 A
Current phase	$15°$	$16°$
Rotational speed	$1,500 \, \text{min}^{-1}$	$1,500 \, \text{min}^{-1}$
Output torque	5.57 N m	5.97 N m
Torque ripple	6.8 %	6.1 %
Output power	874.9 W	937.7 W
Loss in cores	47.2 W	46.0 W
Loss in magnets	1.2 W	0.7 W
Loss in windings	30.0 W	30.0 W
Efficiency	91.8 %	92.4 %

the fundamental, 5th, and 7th space harmonics generate as dominant space harmonics. The 5th space harmonic produces the drive torque and the other space harmonics increase losses without contributing to torque production. In terms of the motor performance, the slit stator improves the space harmonic distribution. In the conventional motor, the space harmonics whose order is a multiple of 3 appear due to the magnetic saturation at the yoke shown in Fig. 2.

The performance is improved by the slit stator. Table 2 presents the performance of the slit stator motor and the conventional motor at an operation with a fed current of 10 A and $1,500 \, \text{min}^{-1}$. The current phase is adjusted to maximise the output torque for each motor. The slit stator motor produces higher torque than the conventional motor with the identical input current. This is due to the increased 5th space harmonic in the air-gap flux density distribution. The slit stator shifts the current phase for maximising the torque by $1°$ because the slits increase the difference between the q-axis and the d-axis inductances. The losses in cores and magnets are
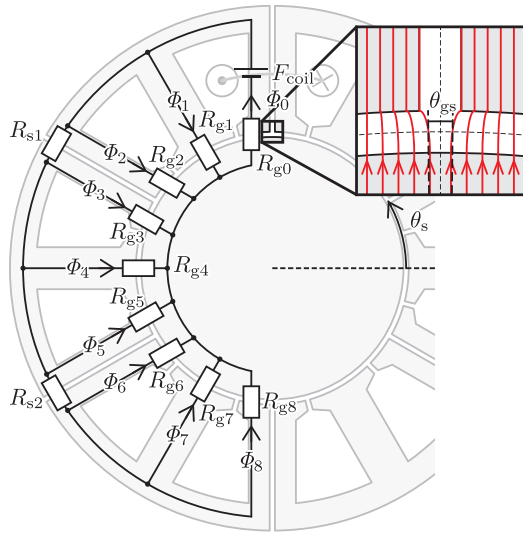
Fig. 4: Magnetic circuit associated with a coil side in a slit stator motor

decreased by the slit stator. This is mainly due to the decreased fundamental and 7th space harmonics. In addition, torque ripple is little influenced by the insertion of slits because of the fractional slot-pole combination and the interior permanent magnet rotor structure. Therefore, the enhanced performance is due to the space harmonic distribution improved with the slit stator.

3 Magnetic Circuit Model

This section describes a magnetic circuit model to theoretically estimate the spatial distribution of the air-gap flux density in a slit stator motor. The rotor is modelled as an iron core that does not have a shaft, magnets, or magnet insertion holes to remove the influence of the rotor structure. The magnetic resistance of cores is assumed to be negligible. The influences of the axial flux and the slot opening are neglected on the air-gap flux density distribution.

The magnetic circuit associated with a coil side, which is designated as U1P, can be modelled for half of the motor, as shown in Fig. 4. The magnetomotive force F_{coil} is generated by the phase current I through the coil side:

$$F_{\text{coil}} = N_{\text{coil}} I, \qquad (1)$$

where N_{coil} denotes the number of turns for each coil. Magnetic resistances appear at the air gap between the stator and the rotor and at the slits. For each integer i, the flux Φ_i passes through the magnetic resistance $R_{\text{g}i}$. The magnetic resistances, which are designated as $R_{\text{g}0}$, $R_{\text{g}2}$, $R_{\text{g}3}$, $R_{\text{g}5}$, $R_{\text{g}6}$, and $R_{\text{g}8}$, are modelled for the air gap on the flux passes through half of slit teeth and expressed by

$$R_{\text{g}i} = \frac{2l_{\text{g}}}{\mu_0 L d_{\text{g}}(\pi/12 - \theta_{\text{gs}}/2)}, \quad \text{for } i = 0, 2, 3, 5, 6, 8, \qquad (2)$$

where μ_0 is the permeability of vacuum, l_{g} denotes the length of the air gap, and L represents the stack length. The diameter of the air gap d_{g} is defined as the sum of the rotor outer diameter d_{r} and the air gap length l_{g} or $d_{\text{g}} = d_{\text{r}} + l_{\text{g}}$. The angle θ_{gs} denotes the equivalent angular width of slits to reduce the width of flux passes across the air gap, as shown in Fig. 4. The equivalent angular slit width θ_{gs} can be written by

$$\theta_{\text{gs}} = \frac{2}{d_{\text{r}} + 2l_{\text{g}}} \left\{ w - 2l_{\text{g}} \log \left(\frac{(w/2) + \sqrt{(w/2)^2 + l_{\text{g}}^2}}{l_{\text{g}}} \right) \right\}. \qquad (3)$$

The magnetic resistances, which are designated as $R_{\text{g}1}$, $R_{\text{g}4}$, and $R_{\text{g}7}$, are modelled for the air gap on the flux passes through

unwound teeth and expressed by

$$R_{\text{g}i} = \frac{2l_{\text{g}}}{\mu_0 L d_{\text{g}}(\pi/6)}, \quad \text{for } i = 1, 4, 7. \qquad (4)$$

The magnetic resistances, which are designated as $R_{\text{s}1}$ and $R_{\text{s}2}$, are defined for the slits and expressed by

$$R_{\text{s}1} = R_{\text{s}2} = R_{\text{s}} = \frac{2w}{\mu_0 L(d_{\text{s}} - d_{\text{r}} - 2l_{\text{g}})}, \qquad (5)$$

where d_{s} denotes the stator outer diameter.

The spatial distribution of the air-gap flux density is calculated from the magnetic circuit. The fluxes are obtained as

$$\Phi_0 = \frac{2R_{\text{g}12}R_{\text{g}345} + R_{\text{g}12}R_{\text{s}} + R_{\text{g}345}^2 + 3R_{\text{g}345}R_{\text{s}} + R_{\text{s}}^2}{X} F_{\text{coil}}, \qquad (6)$$

$$\Phi_{12} = \Phi_1 + \Phi_2 = \frac{R_{\text{g}345}^2 + 3R_{\text{g}345}R_{\text{s}} + R_{\text{s}}^2}{X} F_{\text{coil}}, \qquad (7)$$

$$\Phi_{345} = \Phi_3 + \Phi_4 + \Phi_5 = \frac{R_{\text{g}12}R_{\text{g}345} + R_{\text{g}12}R_{\text{s}}}{X} F_{\text{coil}}, \qquad (8)$$

and

$$\Phi_{678} = \Phi_6 + \Phi_7 + \Phi_8 = \frac{R_{\text{g}12}R_{\text{g}345}}{X} F_{\text{coil}}, \qquad (9)$$

where X, $R_{\text{g}12}$, and $R_{\text{g}345}$ are defined as

$$\begin{aligned} X = {} & 2R_{\text{g}0}R_{\text{g}12}R_{\text{g}345} + R_{\text{g}0}R_{\text{g}12}R_{\text{s}} \\ & + R_{\text{g}0}R_{\text{g}345}^2 + 3R_{\text{g}0}R_{\text{g}345}R_{\text{s}} + R_{\text{g}0}R_{\text{s}}^2 \\ & + R_{\text{g}12}R_{\text{g}345}^2 + 3R_{\text{g}12}R_{\text{g}345}R_{\text{s}} + R_{\text{g}12}R_{\text{s}}^2, \end{aligned} \qquad (10)$$

$$\frac{1}{R_{\text{g}12}} = \frac{1}{R_{\text{g}1}} + \frac{1}{R_{\text{g}2}}, \qquad (11)$$

and

$$\frac{1}{R_{\text{g}345}} = \frac{1}{R_{\text{g}3}} + \frac{1}{R_{\text{g}4}} + \frac{1}{R_{\text{g}5}} = \frac{1}{R_{\text{g}6}} + \frac{1}{R_{\text{g}7}} + \frac{1}{R_{\text{g}8}}, \qquad (12)$$

respectively. For the static angular coordinate θ_{s}, as defined in Fig. 4, the spatial distribution of the air-gap flux density due to the current of the coil side, which is designated as U1P, is obtained as

$$B_{\text{U1P}}(\theta_{\text{s}}) = \begin{cases} \dfrac{2\Phi_0}{L d_{\text{g}}(\pi/12 - \theta_{\text{gs}}/2)}, \\ \quad \text{if } \pi/2 + \theta_{\text{gs}}/2 \leq \theta_{\text{s}} < 7\pi/12, \\[4pt] \dfrac{2\Phi_{12}}{L d_{\text{g}}(\pi/4 - \theta_{\text{gs}}/2)}, \\ \quad \text{if } 7\pi/12 \leq \theta_{\text{s}} < 5\pi/6 - \theta_{\text{gs}}/2, \\[4pt] \dfrac{2\Phi_{345}}{L d_{\text{g}}(\pi/3 - \theta_{\text{gs}})}, \\ \quad \text{if } 5\pi/6 + \theta_{\text{gs}}/2 \leq \theta_{\text{s}} < 7\pi/6 - \theta_{\text{gs}}/2, \\[4pt] \dfrac{2\Phi_{678}}{L d_{\text{g}}(\pi/3 - \theta_{\text{gs}})}, \\ \quad \text{if } 7\pi/6 + \theta_{\text{gs}}/2 \leq \theta_{\text{s}} < 3\pi/2 - \theta_{\text{gs}}/2, \\[4pt] 0, \quad \text{otherwise.} \end{cases}$$

$$(13)$$

Therefore, the spatial distribution of the air-gap flux density due to the stator winding current can be obtained from the superposition of those due to all the coil sides in the stator windings. Space harmonics can be calculated as the Fourier coefficients of the obtained spatial distribution for each harmonic order.

The influences of the slit width are generally estimated from the magnetic circuit model on the space harmonics. Each space harmonic B_ν whose harmonic order is ν is expressed as the function
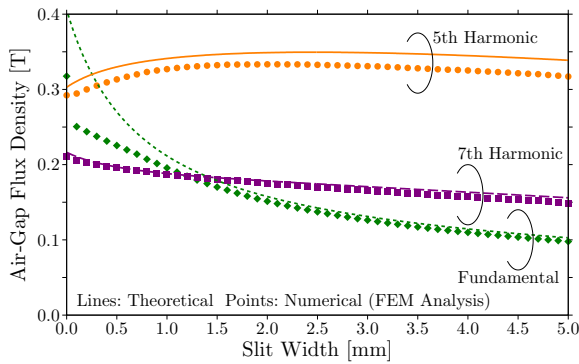
a
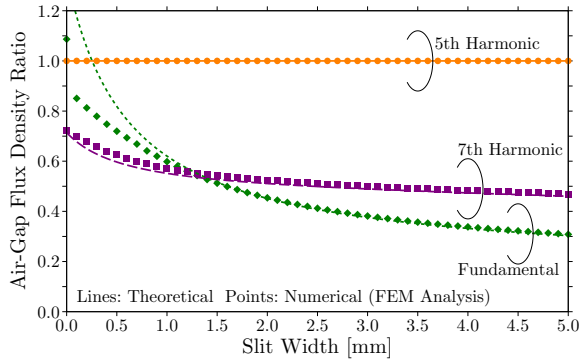
b

Fig. 5: Dominant space harmonics in the air-gap flux density distribution for the slit width at a fed current of $10\,\mathrm{A}$ in the slit stator motor

a Amplitude

b Amplitude ratio

of the slit width w. The fundamental and the 7th space harmonics $B_1(w)$ and $B_7(w)$ monotonically decrease with the increase of the slit width as the following inequalities:

$$\frac{\mathrm{d}B_1(w)}{\mathrm{d}w} < 0\,\mathrm{T/m} \quad \text{and} \quad \frac{\mathrm{d}B_7(w)}{\mathrm{d}w} < 0\,\mathrm{T/m}. \qquad (14)$$

The 5th space harmonic $B_5(w)$ satisfies the following inequalities:

$$\left.\frac{\mathrm{d}B_5(w)}{\mathrm{d}w}\right|_{w=0\,\mathrm{m}} > 0\,\mathrm{T/m} \quad \text{and} \quad \left.\frac{\mathrm{d}B_5(w)}{\mathrm{d}w}\right|_{w\gg0\,\mathrm{m}} < 0\,\mathrm{T/m}. \qquad (15)$$

These inequalities clarify that the 5th space harmonic is maximised at a finite width of slits. Therefore, the space harmonic distribution can be improved by adjusting the slit width.

4 Design of Slit Width

The slit width is determined theoretically and numerically to improve the space harmonic distribution of the air-gap flux density as the most essential design of the slit-like flux barriers in the slit stator motor. The dimensions of the analysed motor are fixed at the values presented in Table 1. The yoke depth differs according to the presence or absence of slits. The rotor is modelled as an iron core that does not have a shaft, magnets, or magnet insertion holes in the magnetic circuit model and the 2D FEM analysis.

The influence of the slit width on the dominant space harmonics is investigated at a fed current of $10\,\mathrm{A}$ through the theoretical calculation based on the magnetic circuit model and the FEM analysis, as shown in Fig. 5. The lines correspond to the theoretical results and the points the numerical results. The numerical results are qualitatively consistent with the theoretical ones. The 5th space harmonic
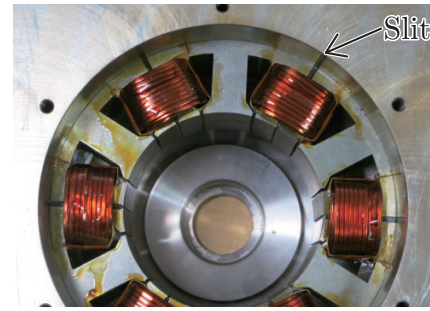
is maximised at a finite width of slits, namely, at $2.5\,\mathrm{mm}$ in the theoretical method and at $2.0\,\mathrm{mm}$ in the numerical one, in Fig. 5a. The fundamental and 7th space harmonics are decreased with the increase of the slit width. The theoretical calculation estimates the dominant space harmonics to be higher than the FEM analysis. This is caused by the assumptions that the magnetic resistance of cores and the influence of the slot opening are neglected in the theoretical method. These results clarify that the slit stator design can increase the 5th space harmonic and decrease the fundamental and 7th space harmonics. However, the increase of the slit width does not necessarily enhance the 5th space harmonic. The wide slits cause the flux density drops at the air gap faced by the slits. The flux density drop can be confirmed at $90°$ and $270°$ in Fig. 3a. Fig. 5b shows the ratio of the dominant space harmonics to the 5th space harmonic. From this figure, it is confirmed that the 5th space harmonic decreases gradually in comparison with the other harmonics for a slit width that is greater than $2.0\,\mathrm{mm}$. For this reason, the slit width can be greater than $2.0\,\mathrm{mm}$ to improve the space harmonic distribution.

The design of the slit width is restricted by the dimensions of slots. The insertion of slits decreases the area of slots. On the other hand, the slit stator has a narrower yoke than the conventional one. The narrower yoke contributes to the increase of the slot area. Therefore, the slit width should be designed less than $2.7\,\mathrm{mm}$ not to decrease the slot area from that of the conventional motor.

5 Experimental Verification

The improved air-gap flux density distribution is verified through an experiment performed with a prototype, as shown in Fig.6. The slit width of the prototype is determined at $2.5\,\mathrm{mm}$. In the prototype, the gap corresponding to each slit is maintained by inserting a nonmagnetic material plate. Both ends of each slit have a gap of $1.5\,\mathrm{mm}$ to fix the plate in the radial direction, as shown in Fig. 7. It is noted that this slightly changes the space harmonic distribution of the air-gap flux density.

Fig. 6: Stator of the prototype

5.1 Measurement Method

The distribution of the air-gap flux density is measured with a search coil wound around a dedicated rotor in this paper. Fig. 7 shows the structure of the measuring rotor with the search coil. The rotor has no magnets, no magnet insertion holes, and two slots for the search coil. The slot pitch is $180°$ mechanical to measure the fundamental space harmonic and odd-order space harmonics in the air-gap flux density distribution. Stationary terminals of the search coil are established with slip rings.

The spatial distribution of the air-gap flux density is acquired as the temporal distribution of a voltage induced in the search coil with the measuring rotor rotating. The two distributions are related as follows. The spatial distribution of the air-gap flux density $B(\theta_s)$, where θ_s is the static angular coordinate defined in Fig. 7, is generated by a static stator winding current. It is assumed that $B(\theta_s + \pi) = -B(\theta_s)$ because of the winding arrangement. The measuring rotor is rotated at an angular velocity ω. The rotor position θ is defined as the difference between the winding axes of the
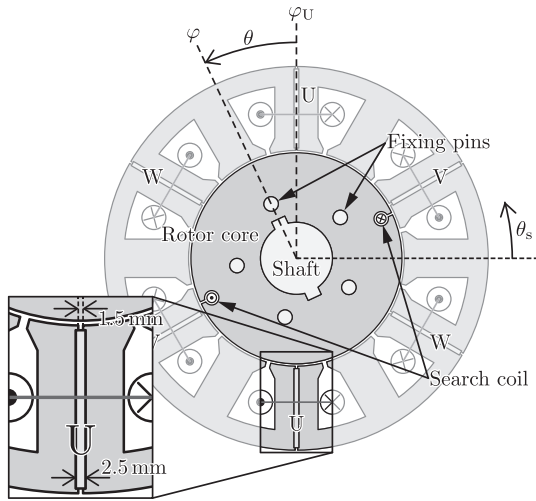
Fig. 7: Cross sections of the measuring rotor at a rotor position of θ and an enlarged slit tooth

search coil φ and the U-phase winding coils φ_U or $\theta = \varphi - \varphi_U = \varphi - \pi/2$. For a rotor position θ, the flux linkage of the search coil is expressed by

$$\phi(\theta) = N \int_{\varphi-\pi/2}^{\varphi+\pi/2} \frac{1}{2} L d_g B(\theta_s) \, d\theta_s$$
$$= N \int_{\theta}^{\theta+\pi} \frac{1}{2} L d_g B(\theta_s) \, d\theta_s, \tag{16}$$

where N denotes the number of turns for the search coil, d_g the diameter of the air gap, and L the stack length. Then, the voltage $e(t)$ induced in the search coil is written as

$$e(t) = \frac{d\phi(\theta)}{dt} = \omega \frac{d\phi(\theta)}{d\theta}. \tag{17}$$

Substitution of (16) into (17) derives

$$e(t) = \frac{1}{2} \omega N L d_g \left\{ B(\theta + \pi) - B(\theta) \right\}$$
$$= -\omega N L d_g B(\theta). \tag{18}$$

Hence, the spatial distribution of the air-gap flux density is acquired as the temporal distribution of the induced voltage based on the relation (18).

5.2 Measured Results

The distribution of the air-gap flux density is measured by rotating the measuring rotor at $1,500 \, \text{min}^{-1}$. The other parameters are set at $N = 10$, $d_g = 89 \, \text{mm}$, and $L = 50 \, \text{mm}$. The fed current is set at $10 \, \text{A}$ and the phase is adjusted to maximise the U-phase current. The measured voltage has been converted into the corresponding air-gap flux density through the relation (18).

The measured air-gap flux density distribution and its harmonic components are shown in Fig. 8. For comparison, numerical results through a 3-dimensional FEM analysis are shown for the conventional motor and the slit stator motor whose rotor is modelled as an iron core with a shaft and fixing pins at a rotor position of $\theta = 0 \, \text{rad}$, as shown in Fig. 7. The experimental result is almost consistent with the numerical result of the slit stator motor. The difference is mainly caused by a fabrication error of the slit stator because the stator is composed of 6 tooth cores and 6 pairs of slit tooth cores. The experimental and numerical results exhibit a similar tendency of space harmonic distribution in the slit stator motor in comparison with that in the conventional one although these results have the difference.
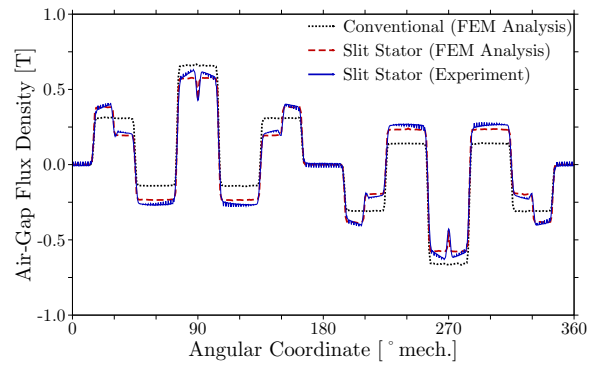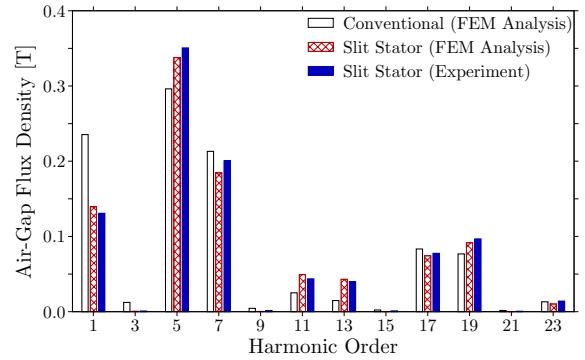
Fig. 8: Air-gap flux density at a fed current of $10 \, \text{A}$ measured for the prototype and calculated for the conventional motor and the slit stator motor with a slit width of $2.5 \, \text{mm}$
a Spatial distribution
b Harmonic components

The improved space harmonic distribution of the air-gap flux density is verified with the experimental and numerical results. The measurement method can estimate the spatial distribution of the air-gap flux density.

6 Conclusion

In this paper, the width of the slit-like flux barriers is designed to improve the space harmonic distribution of the air-gap flux density in a slit stator motor. The influence of the slit width on the space harmonic distribution is investigated through a theoretical calculation based on a magnetic circuit model and an FEM analysis. The theoretical method clarifies that a finite width of slits can improve the space harmonic distribution for the following reasons. The space harmonic producing the drive torque or the 5th space harmonic is maximised at a finite width of slits. The other dominant detrimental space harmonics or the fundamental and the 7th space harmonics are decreased with the increase of the slit width. The numerical results through the FEM analysis are qualitatively consistent with the theoretical ones. The slit width is determined at $2.5 \, \text{mm}$ for a prototypes. The space harmonic distribution improved at a slit width of $2.5 \, \text{mm}$ is verified by performing an experiment with a measuring rotor. The slit stator design can increase the manufacturing cost and decrease the mechanical strength. The prototype has adequate mechanical strength due to the robust frame. These problems can be solved by refining the shape of the slit-like flux barriers in the future.

7 Acknowledgments

8 References

1 Ishak, D., Zhu, Z.Q., Howe, D.: 'Eddy-current loss in the rotor magnets of permanent-magnet brushless machines having a fractional number of slots per pole', IEEE Trans. Magn., 2005, 41, (9), pp. 2462–2469

2 Bianchi, N., Fornasiero, E.: 'Index of rotor losses in three-phase fractional-slot permanent magnet machines', IET Electr. Power Appl., 2009, 3, (5), pp. 381–388

3 Bianchi, N., Bolognani, S., Fornasiero, E.: 'An overview of rotor losses determination in three-phase fractional-slot PM machines', IEEE Trans. Ind. Appl., 2010, 46, (6), pp. 2338–2345

4 Li, J., Choi, D. W., Son, D.H., et al.: 'Effects of MMF harmonics on rotor eddy-current losses for inner-rotor fractional-slot axial flux permanent magnet synchronous machines', IEEE Trans. Magn., 2012, 48, (2), pp. 839–842

5 Fornasiero, E., Bianchi, N., Bolognani, S.: 'Slot harmonic impact on rotor losses in fractional-slot permanent-magnet machines', IEEE Trans. Ind. Electr., 2012, 59, (6), pp. 2557–2564

6 Kometani, H., Asao, Y., Adachi, K.: 'Dynamo-electric machine', U.S. Patent, 2000, 6,166,471

7 Ito, K., Naka, K., Nakano, M., et al.: 'Electric machine', U.S. Patent, 2009, 7,605,514 B2

8 Cistelecan, M.V. , Ferreira, F.J.T.E., Popescu, M.: 'Three phase tooth-concentrated multiple-layer fractional windings with low space harmonic content', Proc. IEEE ECCE, Atlanta, GA, USA, Sep. 2010, pp. 1399–1405

9 Alberti, L., Bianchi, N.: 'Theory and design of fractional-slot multilayer windings', IEEE Trans. Ind. Appl., 2013, 49, (2), pp. 841–849

10 Alberti, L., Barcaro, M., Bianchi, N.: 'Design of a low-torque-ripple fractional-slot interior permanent-magnet motor', IEEE Trans. Ind. Appl., 2014, 50, (3), pp. 1801–1808

11 Sun, A., Li, J., Qu, R., et al.: 'Effect of multilayer windings on rotor losses of interior permanent magnet generator with fractional-slot concentrated windings', IEEE Trans. Magn., 2014, 50, (11), 8105404

12 Bianchi, N., Alberti, L., Barcaro, M.: 'Design and tests of a four-layer fractional-slot interior permanent-magnet motor', IEEE Trans. Ind. Appl., 2016, 52, (3), pp. 2234–2240

13 Ishak, D., Zhu, Z.Q., Howe, D.: 'Permanent-magnet brushless machines with unequal tooth widths and similar slot and pole numbers', IEEE Trans. Ind. Appl., 2005, 41, (2), pp. 584–590

14 Cheng, S.P., Hwang, C.C.: 'Design of high-performance spindle motors with single-layer concentrated windings and unequal tooth widths', IEEE Trans. Magn., 2007, 43, (2), pp. 802–804

15 Dajaku, G., Gerling, D.: 'Low costs and high-efficiency electric machines', Proc. EDPC, Nuremberg, Germany, Oct. 2012

16 Dajaku, G., Xie, W., Gerling, D.: 'Reduction of low space harmonics for the fractional slot concentrated windings using a novel stator design', IEEE Trans. Magn., 2014, 50, (5), 8201012

17 Li, G.J., Zhu, Z.Q., Foster, M., et al.: 'Comparative studies of modular and unequal tooth PM machines either with or without tooth tips', IEEE Trans. Magn., 2014, 50, (7), 8101610

18 Yokoi, Y., Higuchi, T.: 'Design analysis of slit stator motors', Proc. ICEMS, Chiba, Japan, Nov. 2016

19 Yokoi, Y., Higuchi, T.: 'Stator slitting of 12-slot 10-pole concentrated winding motors', IEEE Trans. Ind. Appl., 2018, 54, (5), pp. 4377–4385

20 Yokoi, Y., Hashizume, R., Higuchi, T.: 'Design of slit-like flux barriers to improve space harmonic distribution in a slit stator motor', Digest of INTERMAG, Singapore, Apr. 2018, pp. 213–214